Coupling between cw lasers and a frequency comb in dense atomic samples

2010 J. Phys. B: At. Mol. Opt. Phys. 43 055001

(http://iopscience.iop.org/0953-4075/43/5/055001)

J. Phys. B: At. Mol. Opt. Phys. **43** (2010) 055001 (9pp) doi:10.1088/0953-4075/43/5/055001

Coupling between cw lasers and a frequency comb in dense atomic samples

M Polo, C A C Bosco[1], L H Acioli, D Felinto and S S Vianna

Departamento de Física, Universidade Federal de Pernambuco, 50670-901 Recife, PE, Brazil

E-mail: vianna@ufpe.br

Received 11 October 2009, in final form 5 December 2009
Published 16 February 2010
Online at stacks.iop.org/JPhysB/43/055001

Abstract

We report on a detailed investigation of the coupling between a femtosecond-laser frequency comb and a cw diode laser interacting with an atomic medium of variable density. The comb is printed on a Doppler-broadened atomic transition and the frequency-dependent transmission of the cw laser is monitored as it is scanned over the inhomogenously broadened absorption profile. The printing process and its probing are analysed, experimentally and theoretically, as a function of both laser intensities and the atomic density. The results reveal the importance of optical pumping and power broadening by both lasers, allowing us to determine various regimes of competition between them.

1. Introduction

In the last decade, femtosecond (fs) lasers have been established as an essential tool for coherent control, high-resolution spectroscopy and frequency measurements in general, with applications in the fields of biology, chemistry and physics [1–4]. In particular, the new sets of techniques built around the use of the recently developed frequency combs are remarkable for their simplicity [4], all of which may be classified into one of the following categories, according to the use of the fs frequency comb: (i) as a ruler to measure the frequency of a cw laser which interacts with an atomic transition; (ii) as a single direct probe of an atomic transition; and (iii) combined with a cw laser, both interacting with the atomic system. In the present paper we will be interested in the last two techniques, when the frequency comb directly excites the atomic samples. In this case, it is possible to combine the temporal, ultrafast aspect of femtosecond lasers with the spectral resolution of its frequency comb [5], pointing to the future merging of coherent control and high-resolution spectroscopic techniques [6, 7].

Direct excitation of samples by a frequency comb, however, requires a deeper understanding of the various processes responsible for the medium response to the pulse-to-pulse phase change of the femtosecond laser. The study of dilute atomic samples is then essential to this approach, because it allows for a comparison between theory and experiment. Recent examples of such studies include the detailed treatment of the temporal-coherent-control technique in cascade atomic transitions [6, 8], the printing of femtosecond frequency combs in Doppler-broadened atomic vapours [9–13] and high-resolution optical frequency measurements in cold atomic samples [5, 7, 14]. Most of these works consider only the frequency comb exciting the atoms. More recently the idea of printing a population grating in the frequency domain has also been used to obtain high visibilities in the inhomogeneously broadened profile of rare earth ions in solid-state samples with the goal of obtaining multimode solid-state quantum memories [15].

On the other hand, [10–13] introduce a second, cw laser in the experiments in order to probe the action of the femtosecond laser over the various velocity groups of a room-temperature atomic vapour. These studies have revealed situations in which the cw laser has a role beyond that of a simple probe, as in the case where it induces the blurring of the frequency-comb impression in the Doppler profile [13].

Here, we report on a new study on the coupling between cw lasers and a frequency comb. We experimentally investigate this coupling process as a function of atomic density and both laser intensities. The theoretical analysis to model the experimental results reveals the existence of various regimes of competition between the two lasers, depending on their relative intensities and on the nature of the atomic transition (open or closed) excited by the cw laser.

For a better understanding of the physical situation exploited here we recall some of the basic characteristics

[1] Present address: Departamento de Física, Universidade Federal Rural de Pernambuco, 52171-900 Recife, PE, Brazil.

of the interaction of a mode-locked femtosecond laser with an atomic system. This laser delivers a pulse train which has a repetition rate of the order of 100 MHz, corresponding to a pulse-to-pulse temporal separation of tens of ns. The relaxation rate of the atomic medium occurs on a longer time scale. Therefore, the first pulse creates a polarization in the atomic medium which lasts enough to interact with the next pulse. Depending on the relative phase between the medium polarization and the following pulses, interference between them will determine how the atoms are excited. This process leads to an excited state population distributed over the different frequencies within the Doppler profile, and is what we denote as coherent accumulation [6, 9]. We can also understand this process as a kind of Ramsey fringe formation process, with the difference that multiple pulses are responsible for imprinting the frequency comb on the Doppler profile. A classic review on this topic is found in [16], which also deals with two-photon absorption processes. To the lowest order in the diode-laser intensity, this second laser will simply probe the frequency comb imprinted on the atomic medium. As the diode-laser intensity is increased, however, its role in the atomic excitation process becomes important.

In the following, we introduce our experimental setup in section 2 together with the central experimental results. In section 3 we present our model for the experiments of section 2. The goal is to explain the results with the simplest possible model: one that considers the interaction of the two lasers with an ensemble of four-level atoms. We use this model to interpret the blurring of the printed comb as a result of power broadening of the atomic transition by the cw laser. We show that the various velocity groups of atoms are still sensitive to the femtosecond-laser frequency comb, even for high cw-laser powers, but the Stark shift of the atomic transitions by the cw laser displaces the position of the comb teeth in the Doppler profile, around the cw-laser frequency. We also show that open or closed transitions have considerably different behaviours as the cw power is increased, which explains the distortions observed in the comb impressed in the Doppler profile as the atomic density is altered. Finally, in section 4 we present our conclusions.

2. Experiment

A simplified scheme of the experimental setup together with the relevant hyperfine structure of the ^{87}Rb isotope is presented in figure 1. The frequency comb is generated by a mode-locked Ti:sapphire laser (MIRA 900B-Coherent) with a pulse duration of $\approx$ 150 fs and repetition rate of 76 MHz. A home-made external cavity diode laser with a linewidth of about 1 MHz is used as a probe beam. The two beams are overlapped, with orthogonal linear polarizations, forming a small angle at the centre of the sealed Rb vapour cell, in a configuration that can be co- or counter-propagating. The vapour cell is 5 cm long and contains both ^{85}Rb and ^{87}Rb isotopes in their natural abundances, with no buffer gas. The cell is heated in order to control the atomic density, which varies between 10^9 and 10^{12} atoms cm^{-3}.

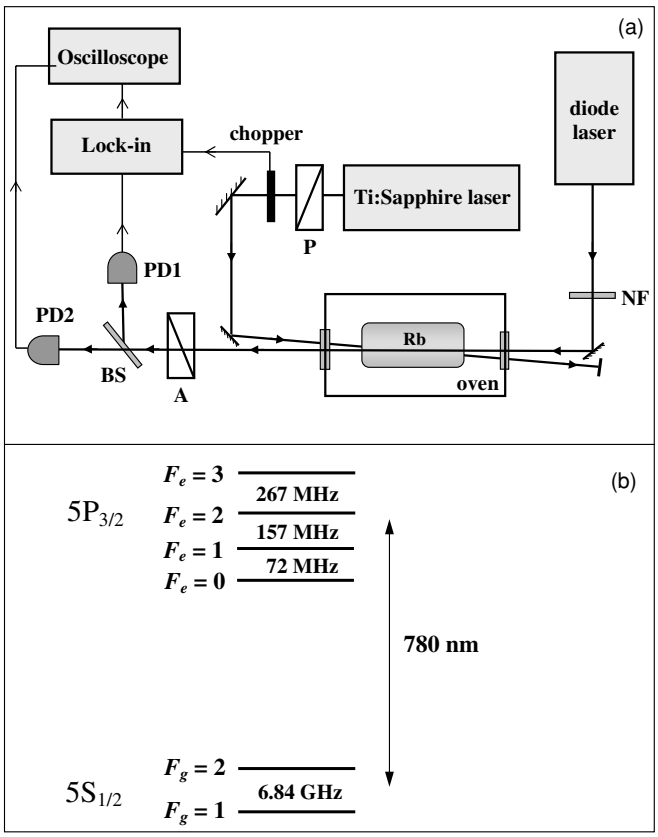

Figure 1. (a) Experimental setup. (b) Relevant energy levels of ^{87}Rb. NF, P, A and BS indicate, respectively, neutral filter, polarizer, analyser, and beam-splitter. PD1 and PD2 are photodetectors 1 and 2, respectively.

The central wavelength of the femtosecond laser is tuned to the ^{87}Rb $5^2S_{1/2} \rightarrow 5^2P_{3/2}$ transition at 780 nm (D_2 resonance line) with a maximum average power of 350 mW and a spectral bandwidth of the order of 8 nm. The average power per mode of the fs laser is of the order of a few μW, and the comb linewidth is negligible compared with the diode-laser linewidth[2]. The fs beam is chopped at 1.8 kHz and focused to a diameter of about 120 μm at the centre of the Rb cell, resulting in a peak electric field of approximately 4.0×10^7 V m^{-1}, which is kept constant in all measurements. The diode-laser beam with a maximum average power of 240 μW is also focused at the centre of the cell with a beam waist of $\approx$100 μm, and its intensity can be varied using neutral-density filters. The probe frequency is scanned across the Doppler-broadened ^{87}Rb $5^2S_{1/2} \rightarrow 5^2P_{3/2}$ hyperfine transitions at a rate of 200 MHz s^{-1}. A saturated absorption setup (not shown) is used to calibrate the probe detuning. The transmission of the cw beam, after passing through cell and a linear analyser, is detected simultaneously with two photodiodes (PD1 and PD2) as a function of its detuning.

[2] The RF linewidth of the repetition rate is much smaller than 10 kHz, limited by our spectrum analyser. Allan deviation measurements give $\sigma_y(\tau) < 10^{-10}$ for observation times τ equal to 1 s. The frequency offset has not been measured but our pump-laser stability ensures that the rms phase deviation is of the order of 10^{-2}–10^{-3} rad for 1 μs, as has been registered for free running ML Ti:sapphire lasers (see [17], for example).

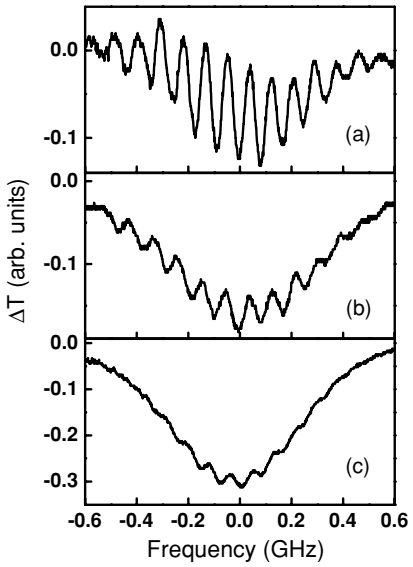

Figure 2. Probe-beam transmission variation (ΔT) as a function of the diode-laser frequency, due to the presence of the fs laser. The diode-laser frequency is scanned over the transitions $5S_{1/2}$ ($F_g = 1$) $\rightarrow$ $5P_{3/2}$ ($F_e = 0, 1, 2$) of ^{87}Rb. Its average power is changed from 4 μW (a), to 80 μW (b), and 240 μW (c). The atomic density is 2.2×10^{10} atoms cm^{-3}.

The signal from photodetector PD1 is processed by a lock-in amplifier employing the chopper frequency as a reference. The lock-in output is monitored and recorded on a digital oscilloscope, together with the signal from photodetector PD2. In this way, whereas the PD2 signal provides the total transmission of the probe beam after passing through the cell, the PD1 signal, after the lock-in, represents the probe-beam transmission variation induced by the fs pulse train. We will denote this transmission variation as $\Delta T = T_{fd} - T_d$, where $T_{fd}(T_d)$ corresponds to the cw-beam intensity at photodetector PD1 when the fs beam is present (absent).

Measurements of the coupling between the two beams for three different diode intensities are displayed in figure 2. Each picture shows the transmission variation of the cw beam induced by the fs pulse train, ΔT, as a function of the diode frequency, when the diode laser scans the ^{87}Rb $5^2S_{1/2}$ ($F_g = 1$) $\rightarrow$ $5^2P_{3/2}$ ($F_e = 0, 1, 2$) hyperfine transitions and the fs laser is tuned to 780 nm. The temperature of the cell is kept constant at 304 K and the two beams are co-propagating through the cell. The average power of the diode beam is (a) 4 μW , (b) 80 μW and (c) 240 μW .

In figure 2(a) we clearly see the frequency comb of the fs laser impressed in the Doppler profile of the Rb atoms. In this situation, where the atomic relaxation times are greater than the laser repetition period, the resonances of the fs-laser field and the atomic system are determined by the frequency comb rather than the spectrum of a single pulse. The modulation observed here is due to the coherent accumulation effect in the excitation process, and is determined by constructive and destructive interferences between the coherences excited by the sequence of pulses from the fs laser [9]. For a weak probe beam, a structure in the modulation can be observed as a direct consequence of a population transfer between the two ground hyperfine levels of Rb induced by the frequency comb. An extensive study of this velocity-selective optical pump (VSOP) process in the D_1 and D_2 lines of Rb and Cs atoms at room temperature was conducted by Pichler's group [10–13].

As the diode power increases, we observe, figures 2(b) and (c), that the visibility of the modulations decreases whereas the absorption of the diode beam induced by the fs laser increases throughout the whole Doppler profile. This behaviour is in agreement with previous experimental results [13].

We also investigate the dependence of the coupling between the two beams with the atomic density. Figure 3 presents the experimental results for four different atomic densities when the two beams are counter-propagating and the average power of the cw beam is kept constant at 4 μW. Each row in figure 3 corresponds to one temperature of the Rb cell, with the two frames in each row obtained simultaneously while the diode laser is scanned across the $F_g = 1 \rightarrow F_e = 0, 1, 2$ transitions of the D_2 line of ^{87}Rb. In the left column we present the signals from photodetector PD1, whereas the signals from photodetector PD2 are present in the right column. The signal from PD2 clearly shows the increase in the absorption of the diode beam as the Rb-cell temperature is increased revealing strong absorption for high temperatures: the diode's intensity after the cell almost vanishes over a large range of frequencies throughout the Doppler profile.

In figure 3(a) we observe the frequency comb of the fs laser impressed in the Doppler profile as in figure 2(a). For these experimental conditions of cw beam intensity and atomic density, ΔT is always negative, indicating that the presence of the fs pulse train leads to an increase of the diode beam absorption for all frequencies in the Doppler profile. As we increase the atomic density, figures 3(b) and (c), we observe positive values for ΔT on the red side of the Doppler profile, indicating decrease in the absorption of the diode beam due to the fs pulse train. For the highest atomic density, on the order of 1.8×10^{12} atoms cm^{-3}, two distinct regions are clearly observed: one with positive values for ΔT on the low-frequency side of the Doppler profile and other with negative values for ΔT on the high-frequency side. The small value of ΔT in the central region is a consequence of the strong absorption of the diode beam for those frequencies.

The results shown in figure 3 indicate that, depending on the atomic density, the fs pulse train plays different roles if the diode frequency is on the blue or red side of the hyperfine transitions. A similar behaviour is also observed for the $F_g = 2 \rightarrow F_e = 1, 2, 3$ transitions of the D_2 line of ^{87}Rb, but in this case, the positive and negative values of ΔT occur on opposite sides with respect to figure 3(d). A comparison of the signal for the transitions from $F_g = 1$ and $F_g = 2$ is shown in figure 4, for the same experimental conditions.

3. Theory

In order to understand the fundamental aspects behind the experimental results of section 2, we consider the simplest possible theory. We model the atom as a four-level system, with two ground states and two excited states (see figure 5).

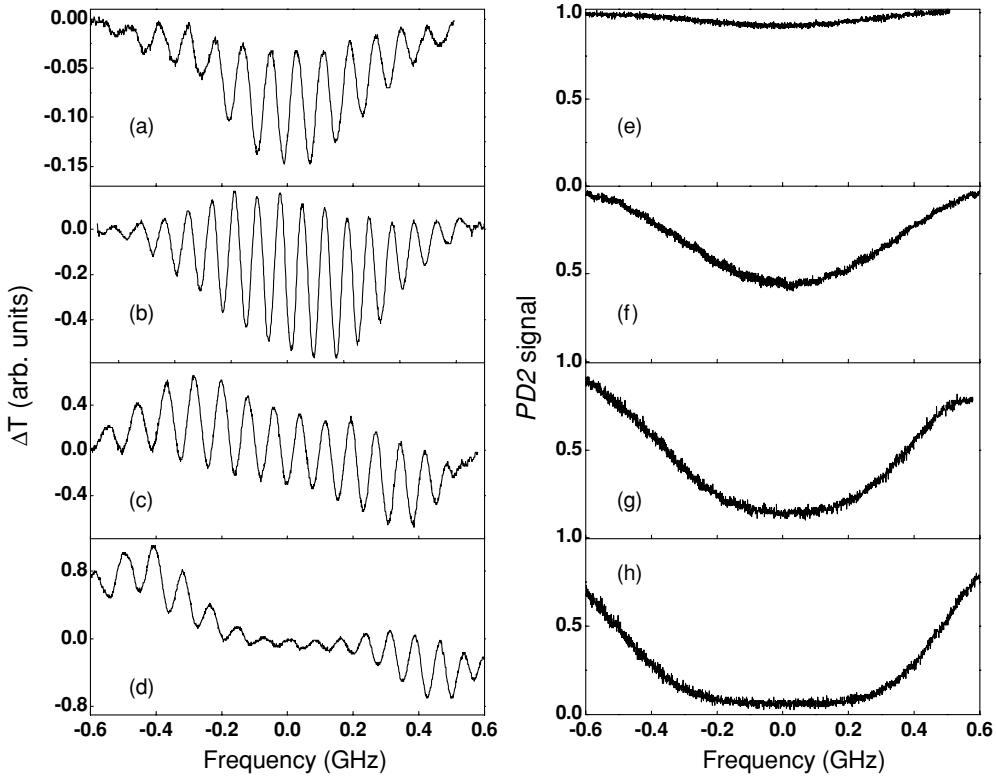

Figure 3. (a)–(d) Probe-beam transmission variation (ΔT) as a function of the diode-laser frequency, due to the presence of the fs laser. (e)–(h) Normalized transmission of the cw diode laser after the cell (PD2 signal) as a function of its frequency. The laser scan parameters are the same as in figure 2. Its average power is 4 μW for all frames. The atomic densities are (a,e) 9.9×10^9 atoms cm^{-3}, (b,f) 3.3×10^{11} atoms cm^{-3}, (c,g) 8.4×10^{11} atoms cm^{-3} and (d,h) 1.8×10^{12} atoms cm^{-3}, respectively.

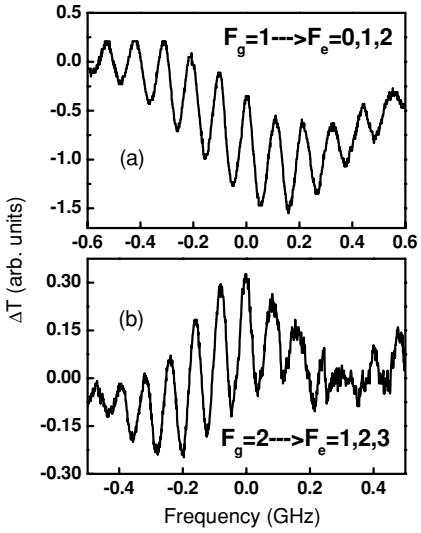

Figure 4. Probe-beam transmission variation (ΔT) as a function of the diode-laser frequency, due to the fs laser. The cw-laser frequency is scanned over all hyperfine transitions starting from (a) $F_g = 1$ and (b) $F_g = 2$ of ^{87}Rb, respectively. The atomic density is 1.8×10^{10} atoms cm^{-3}.

The two ground states, $|1\rangle$ and $|2\rangle$, correspond to the two hyperfine levels of the $5S_{1/2}$ manifold of rubidium. They are essential in the theory in order to allow for the various optical pumping conditions of the system as the experimental parameters are changed. The two excited states, $|3\rangle$ and $|4\rangle$, represent different levels of the $5P_{3/2}$ manifold of rubidium, and are introduced to account for the orthogonal polarizations of the diode and femtosecond lasers. In this way, both lasers may interact with atoms in the same ground state, but, as occurs in the experiment, they do not connect the same transition.

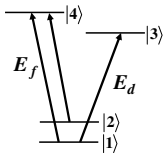

Figure 5. Schematic diagram of the four-level model and the atom–field interactions.

The Hamiltonian of the system is then given by $\hat{H} = \hat{H}_0 + \hat{H}_{\rm int}$, where

$$\hat{H}_0 = \hbar\omega_{12}|2\rangle\langle 2| + \hbar\omega_{13}|3\rangle\langle 3| + \hbar\omega_{14}|4\rangle\langle 4| \qquad (1)$$

represents the Hamiltonian for the free atom, with the transition frequencies $\omega_{ij} = (E_j - E_i)/\hbar$ and E_i the energy of the ith level. The coupling $\hat{H}_{\rm int}$ describing the interaction between each atom and the two lasers is

$$\hat{H}_{\rm int} = -\mu_{13}E_d(t)|1\rangle\langle 3| - \mu_{14}E_f(t)|1\rangle\langle 4| - \mu_{24}E_f(t)|2\rangle\langle 4| + \text{h.c.}, \qquad (2)$$

where μ_{ij} is the dipole moment of the $i \rightarrow j$ transition, and $E_f(t)$ and $E_d(t)$ represent the electric fields for the femtosecond and diode lasers, respectively.

These electric fields can be written as

$$E_d(t) = \mathcal{E}_d(t)\, \mathrm{e}^{\mathrm{i}\omega_d t}, \tag{3a}$$

$$E_f(t) = \mathcal{E}_f(t)\, \mathrm{e}^{\mathrm{i}\omega_f t}, \tag{3b}$$

with $\mathcal{E}_d(t)$ $[\mathcal{E}_f(t)]$ and ω_d $[\omega_f]$ the envelope and central frequency of the diode (femtosecond) laser, respectively. Since we are considering a cw diode laser, we have $\mathcal{E}_d(t) = \mathcal{E}_d$ as a constant. For the train of femtosecond pulses, its envelope can be written as

$$\mathcal{E}_f(t) = \sum_{n=0}^{\infty} \mathcal{E}(t - nT_R)\, \mathrm{e}^{\mathrm{i}n\Phi_R}, \tag{4}$$

with $\mathcal{E}(t)$ the envelope of a single pulse, T_R the repetition period of the laser and Φ_R the round-trip phase acquired by the pulse within the laser cavity [9].

We do not consider the phase fluctuations of the diode and fs lasers in our treatment. These fluctuations occur on a time scale of the order of, or larger than, the time required for the atomic ensemble to reach its stationary state, as will be shown below. The phase fluctuation time scales are given by the inverse of the respective linewidth of a single mode of the lasers, about 1 μs for the diode laser and much larger than that for the fs laser (see footnote 2). During the time evolution to the ensemble's stationary state, the two lasers have a roughly well-defined relative phase, which we consider here, for simplicity, to be zero.

The temporal evolution of the atomic state is given by the set of Bloch equations for the system. In the rotating wave approximation and defining the Rabi frequencies

$$\Omega_d = \frac{\mu_{13}\mathcal{E}_d}{\hbar}, \tag{5a}$$

$$\Omega_{14}(t) = \frac{\mu_{14}\mathcal{E}_f(t)}{\hbar}, \tag{5b}$$

$$\Omega_{24}(t) = \frac{\mu_{24}\mathcal{E}_f(t)}{\hbar}, \tag{5c}$$

the Bloch equations can be written as

$$\frac{\partial\rho_{11}}{\partial t} = (-\mathrm{i}\Omega_{\mathrm{d}}^{*}\sigma_{13} - \mathrm{i}\Omega_{14}^{*}\sigma_{14} + \mathrm{c.c.}) + \frac{\rho_{44}}{2\mathrm{T}_{44}} + \frac{\rho_{33}}{T_{33}}\left(1 - \frac{\Psi}{2}\right) - \gamma\left(\rho_{11} - \rho_{11}^{0}\right), \tag{6a}$$

$$\frac{\partial\rho_{22}}{\partial t} = (-\mathrm{i}\Omega_{24}^{*}\sigma_{24} + \mathrm{c.c.}) + \frac{\rho_{44}}{2\mathrm{T}_{44}} + \frac{\rho_{33}}{\mathrm{T}_{33}}\frac{\Psi}{2} - \gamma\left(\rho_{22} - \rho_{22}^{0}\right), \tag{6b}$$

$$\frac{\partial\rho_{33}}{\partial t} = (-\mathrm{i}\Omega_{\mathrm{d}}\sigma_{31} + \mathrm{c.c.}) - \frac{\rho_{33}}{\mathrm{T}_{33}} - \gamma\rho_{33}, \tag{6c}$$

$$\frac{\partial\rho_{44}}{\partial t} = (-\mathrm{i}\Omega_{14}\sigma_{41} - \mathrm{i}\Omega_{24}\sigma_{42} + \mathrm{c.c.}) - \frac{\rho_{44}}{\mathrm{T}_{44}} - \gamma\rho_{44}, \tag{6d}$$

$$\frac{\partial\sigma_{12}}{\partial t} = \mathrm{i}\omega_{12}\sigma_{12} + \mathrm{i}\Omega_{\mathrm{d}}\sigma_{32} + \mathrm{i}\Omega_{14}\sigma_{42} - \mathrm{i}\Omega_{24}^{*}\sigma_{14} - \gamma\sigma_{12}, \tag{6e}$$

$$\frac{\partial\sigma_{13}}{\partial t} = \mathrm{i}\delta_{\mathrm{d}}\sigma_{13} + \mathrm{i}\Omega_{\mathrm{d}}(\rho_{33} - \rho_{11}) + \mathrm{i}\Omega_{14}\sigma_{43} - \left(\frac{1}{\mathrm{T}_{13}} + \gamma\right)\sigma_{13}, \tag{6f}$$

$$\frac{\partial\sigma_{14}}{\partial t} = \mathrm{i}\left(\delta_{\mathrm{f}} + \frac{\omega_{12}}{2}\right)\sigma_{14} + \mathrm{i}\Omega_{\mathrm{d}}\sigma_{34} + \mathrm{i}\Omega_{14}(\rho_{44} - \rho_{11}) - \mathrm{i}\Omega_{24}\sigma_{12} - \left(\frac{1}{\mathrm{T}_{14}} + \gamma\right)\sigma_{14}, \tag{6g}$$

$$\frac{\partial\sigma_{23}}{\partial t} = \mathrm{i}\left(\delta_{\mathrm{d}} - \omega_{12}\right)\sigma_{23} - \mathrm{i}\Omega_{\mathrm{d}}\sigma_{21} + \mathrm{i}\Omega_{24}\sigma_{43} - \left(\frac{1}{T_{23}} + \gamma\right)\sigma_{23}, \tag{6h}$$

$$\frac{\partial\sigma_{24}}{\partial t} = \mathrm{i}\left(\delta_{\mathrm{f}} - \frac{\omega_{12}}{2}\right)\sigma_{24} - \mathrm{i}\Omega_{14}\sigma_{21} + \mathrm{i}\Omega_{24}(\rho_{44} - \rho_{22}) - \left(\frac{1}{T_{24}} + \gamma\right)\sigma_{24}, \tag{6i}$$

$$\frac{\partial\sigma_{34}}{\partial t} = \mathrm{i}\left(\delta_{\mathrm{f}} - \delta_{\mathrm{d}} + \frac{\omega_{12}}{2}\right)\sigma_{34} + \mathrm{i}\Omega_{\mathrm{d}}^{*}\sigma_{14} - \mathrm{i}\Omega_{14}\sigma_{31} - \mathrm{i}\Omega_{24}\sigma_{32} - \left(\frac{1}{\mathrm{T}_{13}} + \gamma\right)\sigma_{34}, \tag{6j}$$

where ρ_{kl} represents the element kl of the atomic density matrix and T_{kl} represents its relaxation time. The finite interaction time due to the escape of atoms from the interaction region is accounted for by the relaxation rate γ. This loss of atoms is compensated by the arrival of new atoms in the ground state at the same rate. ρ_{11}^{0} and ρ_{22}^{0} are the ground-state populations in thermal equilibrium. The parameter Ψ determines if the $|1\rangle \rightarrow |3\rangle$ transition, driven by the diode laser, is open ($\Psi = 1$) or closed ($\Psi = 0$). The transition is open if the state $|3\rangle$ can decay into either states $|1\rangle$ and $|2\rangle$, and is closed if it only decays into state $|1\rangle$. As we will see, in the case of an open transition, competition between the two lasers is present, depending on their relative intensities, while for a closed transition, the optical pumping process is driven only by the fs laser. The coherences are represented in terms of their slowly varying envelops: $\sigma_{i3} = \rho_{i3}\, \mathrm{e}^{-\mathrm{i}\omega_{\mathrm{d}}\mathrm{t}}$, $\sigma_{i4} = \rho_{i4}\, \mathrm{e}^{-\mathrm{i}\omega_{\mathrm{f}}\mathrm{t}}$, $\sigma_{12} = \rho_{12}$ and $\sigma_{34} = \rho_{34}\, \mathrm{e}^{-\mathrm{i}(\omega_{\mathrm{f}} - \omega_{\mathrm{d}})\mathrm{t}}$ for $i = 1, 2$. The two detunings are defined as $\delta_d = \omega_{13} - \omega_d$ and $\delta_f = \omega_{14} - \omega_{12}/2 - \omega_f$.

The following parameters were used in the numerical calculations: the central frequency of the femtosecond laser was fixed at $\lambda_f = 780$ nm, with pulses of temporal width $T_p = 150$ fs, $\Phi_R = 0$ and a repetition period $T_R = 13$ ns. The lifetimes of the levels $|3\rangle$ and $|4\rangle$, corresponding to two levels of the $5P_{3/2}$ manifold, are taken as $T_{33} = T_{44} = 26.2$ ns. The energy separation between the two ground states $|1\rangle$ and $|2\rangle$ is $\omega_{12}/2\pi = 6835$ MHz [18]. For the homogeneous broadening, we consider only radiative processes and take $T_{13} = T_{14} = T_{23} = T_{24} = T_{34} = 2T_{44} = 52.4$ ns. For a beam waist of ≈ 100 μm, and at room temperature, we consider an interaction time of 400 ns, corresponding to a relaxation rate of $\gamma = 2.5 \times 10^6$ rad s^{-1}.

We also consider an inhomogeneous Doppler broadening of $\delta_D/2\pi = 0.2$ GHz. In this case, the detuning for an arbitrary group of atoms in the Doppler profile can be written as $\delta_d = \delta_d^o - \delta$ and $\delta_f = \delta_f^o \pm \delta$, where δ_f^o (δ_d^o) represents the detuning, relative to the laser frequency ω_f (ω_d), for a group of atoms at rest in the laboratory frame. The plus (minus) sign corresponds to the situation where the two lasers are counter-propagating (co-propagating). δ is the Doppler detuning with respect to the centre of the distribution and labels the different

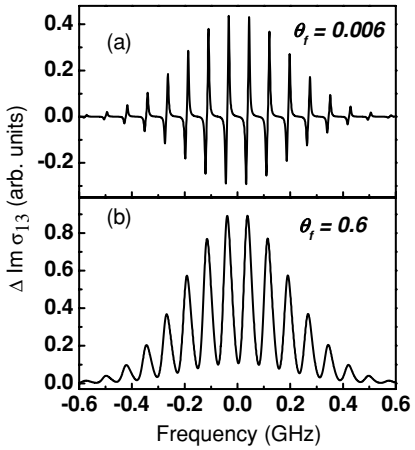

Figure 6. Calculated probe-beam transmission variation ($\Delta\mathrm{Im}\sigma_{13}$) as a function of the diode-laser frequency, in the presence of the fs laser. We consider a weak cw field, $\theta_d = 5 \times 10^{-5}$ acting on the open $|1\rangle \rightarrow |3\rangle$ transition, and two intensities of the fs laser.

groups of atoms within the Doppler profile. As the fs-laser frequency is fixed in the experiment, we arbitrarily consider $\delta_f^o = 0$ in the numerical calculations.

The time evolution of the atomic populations and coherences is obtained by solving the set of coupled differential equations, equations (6), for all orders of the fields. The Bloch equations were integrated using a standard fourth-order Runge–Kutta method with adaptive step size [19]. For the numerical calculations, we consider a train of pulses interacting with an atom initially in the ground state, with $\mu_{13} = \mu_{14} = \mu_{24} = 1 \times 10^{-29}$ C m (average electric dipole moment for the D_2 line) and $\rho_{11}^o = \rho_{22}^o = 0.5$.

We start by considering the weak-field limit for both fs and cw lasers and investigate the effect of increasing the fs-laser intensity on the diode-laser transmission. In sections 3.1 and 3.2 we investigate the variation of the cw-laser power and the dependence on the atomic density, respectively.

To compare with our experimental results we first note that the probe-beam transmission variation is related to the absorption of the diode beam by the medium. The average power lost by the probe beam per unit volume is [20]

$$\frac{\overline{\text{Power}}}{\text{Volume}} = \overline{\mathbf{E}_d \cdot \frac{\partial \mathbf{P}_d}{\partial t}}, \tag{7}$$

where $\mathbf{P}_d$ is the total electric polarization of the atomic medium at the diode-laser frequency. For an ensemble of atoms, the absorption is therefore given by the imaginary part of the polarization, which is proportional to the coherence between the levels $|1\rangle$ and $|3\rangle$, σ_{13}, excited by the diode laser. As we measure the probe-beam transmission variation induced by the fs pulse train, we calculate $\Delta\mathrm{Im}\sigma_{13} = -\left(\mathrm{Im}\sigma_{13}^{\mathrm{fd}} - \mathrm{Im}\sigma_{13}^{\mathrm{d}}\right)$, where $\mathrm{Im}\sigma_{13}^{\mathrm{fd}}$ $\left(\mathrm{Im}\sigma_{13}^{\mathrm{d}}\right)$ is the imaginary part of σ_{13} with (without) the presence of the fs beam.

The calculations are performed for different atomic velocity groups (different detunings δ). For each value of δ, the coherences $\sigma_{13}^{\mathrm{fd}}$ and σ_{13}^{d} are evolved up to a time around $\tau = 1.5$ μs, when the system reaches a stationary state that is repeated with a period T_R [9]. In figure 6 we plot $\Delta\mathrm{Im}\sigma_{13}$ as a function of the diode frequency for an open $|1\rangle \rightarrow |3\rangle$ transition and two fs electric-field peak amplitudes: (a) $\mathcal{E}_f = 4 \times 10^5$ V m^{-1} and (b) $\mathcal{E}_f = 4 \times 10^7$ V m^{-1}. In order to compare the intensity of the two beams we define the quantity

$$\theta_{f(d)} = \int_0^{T_R} \frac{\mu_{ij}\mathcal{E}_{f(d)}}{\hbar}\,\mathrm{d}t, \tag{8}$$

which is a parameter that indicates how strongly the transition is driven during one repetition period of the laser. Note that θ_f is the pulse area of a single fs-laser pulse [21]. θ_d has a similar interpretation if we consider the cw laser acting during a period T_R as a square pulse of constant amplitude and duration T_R. In figure 6, the two frames were obtained for fixed cw electric-field amplitude, $\mathcal{E}_d = 0.04$ V m^{-1}, which corresponds to a pulse area of $\theta_d = 5 \times 10^{-5}$. For the fs laser, the pulse areas are (a) $\theta_f = 0.006$ and (b) $\theta_f = 0.6$, respectively.

For each frequency of the cw laser, we take into account only the contribution of the atoms that are on resonance with the diode laser, and weight the curves by the Doppler profile $\exp\left(-\delta^2/2\delta_{\mathrm{D}}^2\right)$. For low femtosecond-laser intensities (figure 6(a)), we clearly observe a velocity selective population transfer between the two lower states, induced by the frequency-comb excitation. As the diode laser only interacts with the ground state $|1\rangle$, we obtain gain or loss depending if the fs laser decreases or increases the population of this state. It means that, for atomic velocity groups for which a tooth of the fs-laser frequency comb is resonant with the $|1\rangle \rightarrow |4\rangle$ transition, the population of level $|1\rangle$ decreases and positive values for $\Delta\mathrm{Im}\sigma_{13}$ are obtained. On the other hand, for atomic velocity groups for which the fs frequency comb is resonant with the $|2\rangle \rightarrow |4\rangle$ transition, population is transferred from level $|2\rangle$ to level $|1\rangle$, increasing the absorption of the cw diode laser and leading to negative values of $\Delta\mathrm{Im}\sigma_{13}$. When the fs-laser intensity increases (figure 6(b)) we continue observing the frequency comb impressed in the Doppler profile, but now, the optical pumping between the two lower states is lost due to power broadening induced by the femtosecond laser [9]. In this case, $\Delta\mathrm{Im}\sigma_{13}$ is always positive due to the high population transfer to level $|4\rangle$ by the fs laser, which decreases the population in level $|1\rangle$ and the overall optical depth of the sample to the diode laser.

3.1. Variation of the cw-laser power

We also investigate the diode-laser transmission variation as its intensity is increased. In the case of a weak fs beam, the calculated fractional population variation is shown in figure 7, for the two ground states, $\Delta\rho_{11}$ (figures 7(a) and (c)) and $\Delta\rho_{22}$ (figures 7(b) and (d)), when the pulse area of the cw beam is smaller or greater than the pulse area of the fs beam. In this figure the fs-laser intensity is fixed at $\theta_f = 0.006$ and the diode electric-field amplitudes are $\mathcal{E}_d = 4$ V m^{-1} (figures 7(a) and (b)) and $\mathcal{E}_d = 5$ V m^{-1} (figures 7(c) and (d)), corresponding to pulse area ratios (θ_d/θ_f) equal to 0.87 and 1.08, respectively. We see that the population of state $|1\rangle$, ρ_{11}, can increase or decrease depending on the relative pulse areas between the two beams, indicating that the strongest beam dominates the optical pumping process. To observe this optical pumping competition between the two beams, we consider a velocity group for which the atoms are resonant simultaneously with the

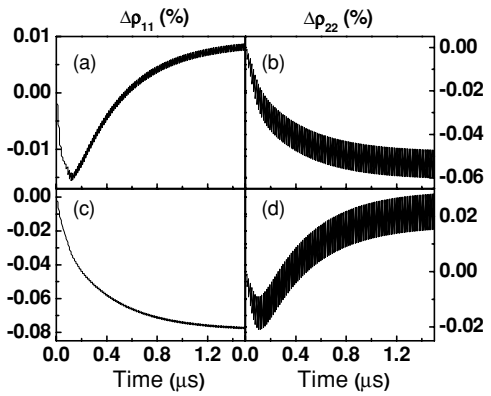

Figure 7. Calculated time evolution of the fractional population variation for $\Delta\rho_{11}$ ((a) and (c)), and $\Delta\rho_{22}$ ((b) and (d)), when the pulse area ratio, (θ_d/θ_f), is <1 for (a) and (b) and >1 for (c) and (d). The curves are obtained for an open diode-laser transition and a velocity group of atoms that is simultaneously resonant with the two beams.

two beams, and perform the calculations for the open diode-laser transition and with the fs frequency-comb resonant with the $|2\rangle \rightarrow |4\rangle$ transition.

Figure 8 shows the population of the excited state, $|4\rangle$, as a function of the atomic velocity distribution for high intensity and fixed frequency of the cw laser. The pulse areas of the two beams are $\theta_f = 0.006$ and $\theta_d = 1.3$. The population distribution, around $\delta = 0$, is displayed for three different conditions: (a) without the diode laser, and with the diode laser exciting (b) a closed and (c) an open transition. The cw diode-laser frequency is fixed at $\omega_d = \omega_{13}$, $(\delta = 0)$ and ρ_{44} is weighted by the Doppler profile. As described previously, the periodic structure with two peaks observed for low-femtosecond-laser intensity (as in figure 6(a)), is a consequence of the two resonant transitions, $|1\rangle \rightarrow |4\rangle$ and $|2\rangle \rightarrow |4\rangle$, with different modes of the fs pulse train. For a diode-laser intensity that corresponds to an electric field amplitude of the order of $\mathcal{E}_d = 1 \times 10^3$ V m^{-1}, we observe that the various atomic velocity groups are still sensitive to the fs-laser frequency comb. However, the Stark shift of the $|1\rangle \rightarrow |3\rangle$ atomic transition by the diode laser displaces the printing of the comb teeth in the Doppler profile which are resonant with the $|1\rangle \rightarrow |4\rangle$ transition, around the cw-laser frequency, as shown in the region around the dashed lines in figure 8. We also note that the comb teeth resonant with the $|2\rangle \rightarrow |4\rangle$ transition are not displaced, as these two levels are not directly connected with the diode laser. Following the dashed lines in figure 8 it is clearly seen that the indicated atomic velocity groups will be resonant or not with the fs-laser frequency comb depending on the cw diode intensity. This means that the accumulative effect observed on the atoms with these specific velocities will be destroyed due to the Stark shift of the atomic transition. On the other hand, as shown in figure 8, there will be other atomic velocity groups that will change from destructive to constructive interference condition, depending on the displacement due to the Stark effect.

A comparison of $\Delta\mathrm{Im}\sigma_{13}$ between an open or closed $|1\rangle \rightarrow |3\rangle$ transition excited by the cw laser is presented in

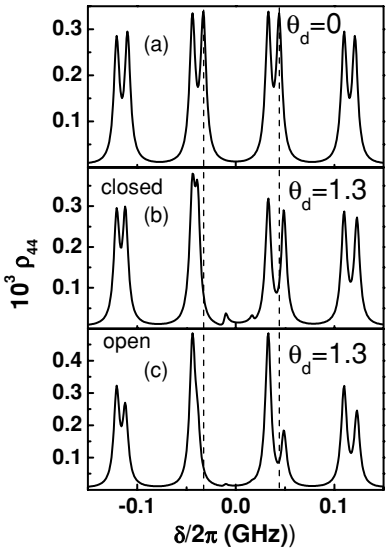

Figure 8. Variation of the population ρ_{44} for different atomic groups, weighted by the Doppler profile and $\theta_f = 0.006$: (a) without the diode laser, and with the diode laser exciting (b) a closed and (c) an open transition. The cw diode-laser frequency is fixed at $\omega_d = \omega_{13}$ $(\delta = 0)$. The dashed lines indicate atomic velocity groups that change from a constructive to destructive interference condition due to the Stark shift.

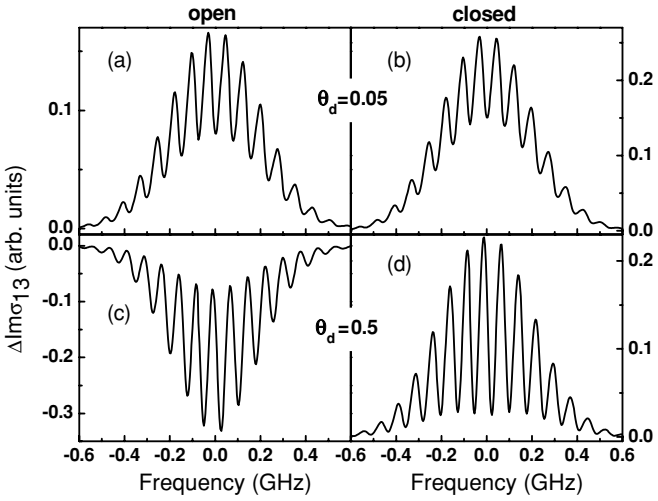

Figure 9. Calculated probe-beam transmission variation of the diode beam $(\Delta\mathrm{Im}\sigma_{13})$ as a function of the cw-laser frequency, due to the fs laser, for open ((a) and (c)) and closed ((b) and (d)) $|1\rangle \rightarrow |3\rangle$ transitions driven by the diode laser and two different cw-laser intensities.

figure 9. The transmission variation of the diode beam induced by the fs laser was calculated for the fixed fs pulse area of $\theta_f = 0.6$, varying the cw-laser pulse area by one order of magnitude: from $\theta_d = 0.05$ $(\mathcal{E}_d = 40$ V m$^{-1})$ ((a) and (b)) to $\theta_d = 0.5$ $(\mathcal{E}_d = 400$ V m$^{-1})$ ((c) and (d)). First, it is important to note that the curve in figure 9(a) was obtained for the same parameters as used in figure 6(b), except for the diode intensity, that is now three orders of magnitude greater. To take into account effects such as power broadening and Stark shift, due to high cw-laser intensity, the curves in figure 9 were obtained integrating, for each position of the diode-laser

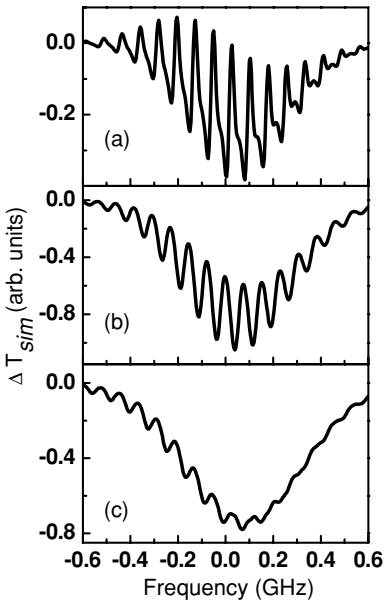

Figure 10. Numerical simulation of the probe-beam transmission variation, $\Delta T_{\rm sim}$, as a function of the diode-laser frequency, due to the fs laser, for three values of the diode electric-field amplitude: $\mathcal{E}_d = 150\ \mathrm{V\,m^{-1}}$, (b) $\mathcal{E}_d = 1 \times 10^3\ \mathrm{V\,m^{-1}}$ and (c) $\mathcal{E}_d = 2 \times 10^3\ \mathrm{V\,m^{-1}}$. The calculations are performed considering all hyperfine transitions from $F_g = 1$.

frequency, the contribution of all atomic velocity groups within the linewidth of the $|1\rangle \rightarrow |3\rangle$ transition. For very low cw-laser intensity, the integration is over the natural linewidth of the transition. However, for the intensities used in figure 9, the integration region must be of the order of the power-broadened linewidth. Comparing figure 6(b) with figure 9(a) we clearly see the blurring of the frequency comb printed in the Doppler profile as a result of the extra power broadening of the atomic transition by the cw laser.

For low cw-laser intensities ($\theta_d \leqslant 0.05$), we obtain amplification of the diode beam induced by the fs beam for both kinds of transitions. As the cw-laser intensity increases, we find an intensity region where the two kinds of transitions, closed and open, present different behaviour with respect to absorption and amplification. While for the closed transition we continue to obtain diode amplification, for the open transition the fs beam induces an increase of the absorption of the diode beam for all frequencies within the Doppler profile. This distinct behaviour can be understood if we note that for the closed transition only the fs beam can transfer population between the states $|1\rangle$ and $|2\rangle$. However, for the open transition, there is a competition between the two lasers in the population transfer process (as shown in figure 7) and the diode laser may prevail when its area is large enough.

To simulate our experimental results, we take into account this distinct behaviour depending on the nature of the atomic transition. The contributions of one closed and two open transitions, $\sum \Delta \mathrm{Im}\sigma_{13}$, are added to calculate the probe-beam transmission variation due to the fs laser, when the cw-laser frequency is scanned over the $F_g = 1 \rightarrow F_e = 0, 1, 2$ hyperfine transitions of the D_2 line of ^{87}Rb. We also consider the frequency separation and the relative transition dipole moments of the hyperfine transitions. In figure 10 we present the simulations for a fs electric-field amplitude of $\mathcal{E}_f = 4 \times 10^7\ \mathrm{V\,m^{-1}}$ ($\theta_f = 0.6$) and three values of the diode electric-field amplitude: (a) $\mathcal{E}_d = 150\ \mathrm{V\,m^{-1}}$ ($\theta_d = 0.2$), (b) $\mathcal{E}_d = 1 \times 10^3\ \mathrm{V\,m^{-1}}$ ($\theta_d = 1.3$) and (c) $\mathcal{E}_d = 2 \times 10^3\ \mathrm{V\,m^{-1}}$ ($\theta_d = 2.5$). These values correspond to the experimental conditions of the results shown in figure 2, at fixed temperature, with an average power of 350 mW for the fs laser and approximately the same ratio between the diode electric-field amplitudes. The curves were obtained by integrating the contribution of all atomic velocity groups within the power-broadened linewidth of the $|1\rangle \rightarrow |3\rangle$ transition, according to each value of the diode electric-field amplitude. Also, for each atomic velocity group, we took the average value, over a period T_R, of the coherences, $\sigma_{13}^{\rm fd}$ and $\sigma_{13}^{\rm d}$, after the system reaches a stationary state. The quantity plotted in figure 10 is the product of $\sum \Delta \mathrm{Im}\sigma_{13}$ and $\Delta \mathcal{E}_d^N$, the diode electric-field amplitude variation due to linear absorption, for each diode frequency. We defined this quantity as $\Delta T_{\rm sim}$, the simulation of the probe-beam transmission variation due to the presence of the fs laser when the cw-laser frequency is scanned over the hyperfine transitions. For low atomic densities as in figure 2, the linear absorption is negligible. To take into account the averaging due to the time constant of the lock-in amplifier we plot the average of $\Delta T_{\rm sim}$ over a range of 20 MHz in the diode frequency. The visibility of the modulations decreases when the diode electric-field amplitude increases, while the absorption of the diode beam induced by the fs laser increases throughout the whole Doppler profile, in good agreement with the experimental results.

3.2. Dependence on the atomic density

The experimental results observed for different atomic densities can be understood qualitatively if we take into account the distinct effects of the open and closed transitions on the changes introduced in the cw beam intensity. First, we note in figures 3(e)–(h) a decrease of the diode beam intensity due to absorption by the rubidium vapour as the atomic density increases. For high cw beam intensity and low atomic densities, however, this decrease is negligible (see figure 3(e)) and the cw beam transmission is also practically frequency independent. Under these conditions, from our theoretical results of section 3.1 (see figure 10), we expect that the open and closed transitions should display the same behaviour, i.e. an increase of the probe beam absorption induced by the fs beam. This is in agreement with the results for the cw-laser frequency scanned over the $F_g = 1 \rightarrow F_e = 0, 1, 2$ hyperfine transitions, as shown in figure 3(a); in fact, negative values for the transmission changes ($\Delta T < 0$) of the cw beam are observed for all frequencies in the Doppler profile.

As the atomic density increases, the cw laser is more absorbed and its intensity decreases in the interaction region, the centre of the cell. Positive values for ΔT are then observed on the red side of the Doppler profile (see figures 3(b)–(d)). As predicted in figure 9, this situation corresponds to an increase of the cw beam transmission induced by the fs beam in the

closed transition, $F_g = 1$ to $F_e = 0$, while negative values for ΔT continue to be observed in the frequency region of the open transitions, $F_g = 1 \rightarrow F_e = 1$ and 2. The influence of the nature of the transition driven by the diode laser is reinforced by the results displayed in figure 4(b) for the cw-laser frequency scanned over the $F_g = 2 \rightarrow F_e = 1, 2, 3$ hyperfine transitions. In this figure, we clearly see that positive values for the probe beam transmission variation appear now on the blue side of the Doppler profile, corresponding again to the frequency region where the closed transition dominates. These features indicate that the distortions observed in the probe-beam transmission variation due to the fs laser and as the atomic density increases (figures 3 and 4) are well explained by the distinct behaviour of these two kinds of transitions driven by the diode laser.

4. Conclusions

In this paper we have presented new results on the coupling between femtosecond-laser frequency combs and a cw diode laser. This coupling process was experimentally investigated when the cw-laser frequency is scanned over the inhomogeneously broadened D_2 resonance line of ^{87}Rb, and the printing of the fs-laser frequency comb in the Doppler profile was studied as a function of the atomic density and laser intensities. We have used the simplest possible model, one that takes into account the interaction of the two lasers with an ensemble of four-level atoms, to explain the experimental results. Our analysis reveals the roles of optical pumping and power broadening in the establishment of the various regimes of competition between the two lasers, depending on their relative intensities and on the nature, if open or closed, of the atomic transition excited by the cw diode laser. We have also shown that the various velocity groups of atoms are sensitive to the femtosecond-laser frequency comb, even for high cw-laser powers, but the Stark shift of the atomic transitions by the cw laser displaces the printing of the comb teeth in the Doppler profile. This result leads to the reinterpretation, with respect to [13], of the blurring of the printed comb as a result of power broadening on the atomic transition by the cw laser. Further, we have shown that open or closed transitions have considerably different behaviours as the cw power is increased, which explains well the distortions observed in the comb printed in the Doppler profile as the atomic density is changed.

Acknowledgments

This work was supported by CNPq, FACEPE and CAPES (Brazilian Agencies).

References

[1] Zewail A H 1994 *Femtochemistry: Ultrafast Dynamics of the Chemical Bonds* (Singapore: Word Scientific)
[2] Rice S A 2000 *Nature* **403** 496 (and references therein)
[3] Udem Th, Holzwarth R and Hansch T W 2002 *Nature* **416** 233
[4] Jun Ye and Cundiff S 2005 *Femtosecond Optical Frequency Comb Technology: Principle, Operation and Application* (Berlin: Springer)
[5] Marian A, Stowe M, Lawall J, Felinto D and Jun Ye 2004 *Science* **306** 2063
[6] Felinto D, Acioli L H and Vianna S S 2004 *Phys. Rev.* A **70** 043403
[7] Stowe M C, Cruz F C, Marian A and Jun Ye 2006 *Phys. Rev. Lett.* **96** 153001
[8] Felinto D, Bosco C A C, Acioli L H and Vianna S S 2001 *Phys. Rev.* A **64** 063413
[9] Felinto D, Bosco C A C, Acioli L H and Vianna S S 2003 *Opt. Commun.* **215** 69
[10] Aumiler D, Ban T, Skenderovic H and Pichler G 2005 *Phys. Rev. Lett.* **95** 233001
[11] Ban T, Aumiler D, Skenderovic H and Pichler G 2006 *Phys. Rev.* A **73** 043407
[12] Vujicic N, Vdovic S, Aumiler D, Ban T, Skenderovic H and Pichler G 2007 *Eur. Phys. J.* D **41** 447
[13] Ban T, Aumiler D, Skenderovic H, Vdovic S, Vujicic N and Pichler G 2007 *Phys. Rev.* A **76** 043410
[14] Marian A, Stowe M C, Felinto D and Jun Ye 2005 *Phys. Rev. Lett.* **95** 023001
[15] Riedmatten H, Afzelius M, Staudt M U, Simon C and Gisin N 2008 *Nature* **465** 773
[16] Salour M M 1978 *Rev. Mod. Phys.* **50** 667
[17] Matos L, Kleppner D, Kuzucu O, Schibli T R, Kim J, Ippen E P and Kaertner F X 2004 *Opt. Lett.* **29** 1683
[18] Steck D A *Rubidium 87 D Line Data* http://steck.us/alkalidata
[19] Press W H, Teukolsky S A, Vetterling W T and Flannery B P 1999 *Numerical Recipes in C: The Art of Scientific Computing* (Cambridge: Cambridge University Press)
[20] Yariv A 1989 *Quantum Electronics* (New York: Wiley)
[21] Allen L and Eberly J 1987 *Optical Resonance and Two-Level Atoms* (New York: Dover)